

NEEDS AND SOLUTIONS FOR MACHINE IMPEDANCE REDUCTION

C. Vollinger*, A. Farricker, T. Kaltenbacher, P. Kramer, B. Popovic
CERN, Geneva, Switzerland

Abstract

Particle beams with highest possible beam intensities are requested nowadays, hence in modern circular accelerators, the consideration of beam coupling impedance issues is of increasing relevance. Classical sources of beam coupling impedance are RF-systems, injection and extraction kickers, but also beam diagnostic elements such as wire scanners where the object itself forms an undesired cavity, and beam pipe transitions, namely tapers or steps. Optimally, for any machine, impedance mitigation shall take place already during the design phase. However, for older existing machines, often considerable hardware changes would be required to obtain a significant impedance reduction. In these cases, the required geometry changes for reducing beam coupling impedance are costly to be carried out, hence retro-fitted solutions such as impedance shields or damping mechanisms are required.

For both approaches, different impedance mitigation strategies are available and their selection also depends on the needs, i.e., the type of problem that is arising. Single bunch instabilities, for example, require an optimization of the object geometry with the goal to reduce R/Q, whereas multi bunch instabilities or heating will ask for different measures. In this presentation, we will explain about typical sources of beam coupling impedances and how they could be circumvented. Possibilities to reduce beam coupling impedance in existing machine elements are included and applied solutions, such as impedance shields or HOM dampers will be presented as well.

INTRODUCTION

The desired operational beam intensity at flat top for the CERN Super Proton Synchrotron (SPS) as injector for high luminosity LHC (HL-LHC) runs is 2.4×10^{11} ppb for a bunch length $\tau = 1.65$ ns and 25 ns spacing [1]. These intensities can be reached only if the interaction of the particle beams with the surrounding structure is known, at least approximately, i.e., a good description of machine elements is required. Known impedance sources are distinguished between machine elements with potentially large individual contribution as, e.g. accelerating cavities and kickers, and other components of which the individual contribution is considered to be small, but which exist in large quantities, such as vacuum valves, beam pipe flanges, vacuum pumping ports, etc. We describe all contributions with a resonator model of a resonant frequency f_{res} , quality factor Q , and a resonant bandwidth Δf , where $Q = \frac{f_{\text{res}}}{\Delta f}$. Considering the type of instability that is triggered by a certain impedance contribution, we can distinguish between **nar-**

rowband impedances for which $\Delta f \ll \frac{1}{\tau}$ and **broadband impedances** for which $\Delta f \gg \frac{1}{\tau}$. If we accept a certain randomness in this division by ignoring the additional dependence on bunch spacing, this allows to categorise our mitigation methods. This way, narrow-band impedances mainly cause coupled bunch instabilities since the resulting wakefield of these resonances remains sufficiently long to affect many bunches. Narrow-band impedances can be reduced by methods that can be denoted as de-Qing, i.e. damping of undesired resonant modes by usually passive means as the introduction of HOM-couplers, or resonance-broadening methods, such as the insertion of absorber ferrites which create losses at a certain frequency. Contrary to this, broadband beam impedances lead only to single bunch instabilities for which usually not the quality factor, but the geometry factor R/Q has to be reduced by changing the overall geometry. This can be obtained either by selecting a suitable geometry for the machine element or by introducing a shield within an existing structure. The usual approach is to calculate the contribution of individual components separately, and once an individual contribution is known, optimisation of this machine element starts. It is, however, well known that this approach is insufficient if the individual elements are coupled to each other. In the following, we will give examples of geometries that appear to be simple, but are electromagnetically complex, as well as how oversimplifications of geometries can give misleading results. Finally, an example is given how in addition to the improvement of individual impedance contributions also the rearrangement of consecutive machine elements can lead to a considerable impedance gain.

MITIGATION ON INDIVIDUAL MACHINE ELEMENTS

Although electron cloud related impedances should not be forgotten since they have been observed in virtually all high energy machines and are typically mitigated by surface treatments as coating or other measures, we will not consider this topic here. Equally, the introduction of absorber ferrites or other lossy material usually comes with the risk of creating a heat-transfer issue if used in vacuum. We will not show such examples here either. Instead, we concentrate on **geometrical changes** since we consider those as the first choice in impedance mitigation, and demonstrate beam impedance mitigation by worked examples taken from the SPS, the last leg in the injector chain for the Large Hadron Collider (LHC). Geometrical changes are usually implemented such that the build-up of resonances is suppressed from the very start, e.g. by reducing the volume of the outer vessel of a machine element to avoid that low frequency resonances build up. In many cases, e.g. for heating issues, it is equally sufficient to

* Christine.Vollinger@cern.ch

shift a critical mode to higher frequencies, hence out of the contributing beam spectrum, e.g. by inserting impedance shields or shorting elements such as bridges, RF-contacts or the like. In addition, HOM-couplers are routinely used to take out resonances in a structure that cannot be avoided from the machine element's geometry, and a detailed worked example is shown in this proceedings in the studies for the 200 MHz travelling wave cavities for the SPS [9]. Finally, as was mentioned already before, using examples also taken from the SPS, we will demonstrate how the re-working of existing machine sections by sorting its individual elements can lead to a considerable reduction of the overall contribution to beam impedance.

Vacuum Pipe Flanges of SPS (Example 1)

The vacuum flanges (VF) in the SPS can be divided in two groups classified by their interconnecting beam pipes [2]. Impedance-wise, the most concerning are circular VF-connections with a bellow attached and connected to flat beam pipe types since those are shaping an unintended pill-box-type cavity with corrugated walls. At the time, the round flanges were chosen, for example, to allow the connection of a rectangular beam-pipe of inner width $w=156$ mm (as is used in the bending magnets MBA-type of the SPS) with a beam-pipe of a quadrupole magnet with the same inner width, but with an elliptical contour. A number of shielding designs can be found for these VFs, all developed with the goal to provide a smooth transition for the different beam pipe shapes. Most of these designs feature RF-contacts, RF-bridges, or both elements, to provide electrical contact between the different parts as well as to the outer VF body, this way, suppressing resonances. These RF-fingers can be completely fixed on both ends, fixed-touching or spring-driven [2] [3], however, their performance depends on a flawless installation that guarantees that the RF-fingers are well-connected. Different from these designs, we were looking for the development of an impedance shield for these VF interconnections that can provide electrical continuity with a maximum mechanical robustness to longitudinal and lateral movements. This type of shield was originally suggested by Ogiwara [4] who also tested different materials as well as different braid-woven patterns for shields [5].

Fig. 1 shows the illustrations of a cut-through of an unshielded VF with bellows (a), and the same vacuum flange with a braided shield fixed on support plates (b). The stainless steel braided shield is highlighted in red. The vacuum flange shield designs have to be compatible with variations in the alignment of the two connecting vacuum chambers, i.e., have to comply to misalignments in the longitudinal as well as in the transverse planes. Fig. 2 visualises how the stainless steel braid (shown in red) can provide smooth continuity by connecting the different beam pipe contours; cut-through (a) and view from the outside (b) with fixed RF-fingers of the support-plate highlighted in yellow. In the case shown, a change of vacuum pipe contour from elliptical QF-type (left side) to rectangular MBA-type (right side) is required. The installation of the stainless steel braid effectively

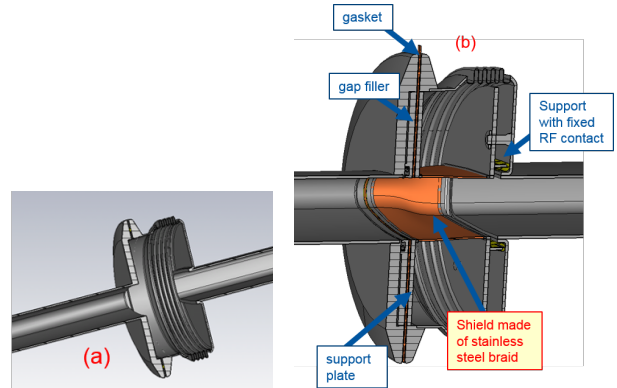


Figure 1: Illustrations of a cut-through of unshielded vacuum flange (VF) with 4-convolution bellows attached (left), and the VF equipped with a braided shield for impedance reduction (right).

suppresses the contribution of the bellows to beam coupling impedance. More details on the braided shield study can be found in a detailed publication [6]. The simulated longitudinal impedance of the SPS vacuum flanges with/without the braided shields is shown in Fig. 3. A comparison of the traces shows that most resonances are effectively suppressed by the shield installation (compare red trace (unshielded VF) to the black trace (with braided shield)). An exception is the resonance at about 1.4 GHz, on which a reduction of impedance contribution and a slight shift of the resonance frequency can be observed. This remaining resonance is building up in the gasket area of the shielded vacuum flanges, where a very flat circular unintended cavity of 2 mm height remains due to the gasket thickness. Consequently, this resonance can be suppressed by closing the gasket gap, e.g. through insertion of a modified gasket shape which will then lead to the blue trace (see [6] for details). Beam dynamics

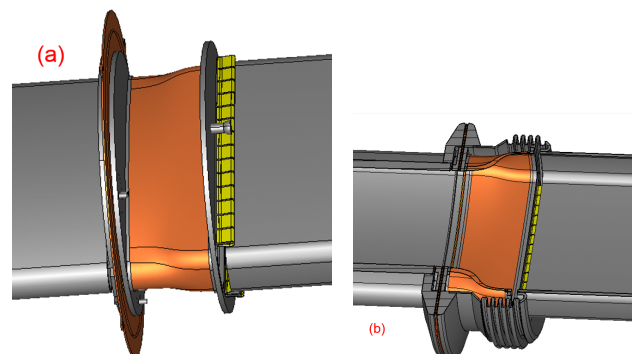


Figure 2: Illustrations of braided shield continuity between different beam-pipe shapes (a), and a cut-through view of braided shield for impedance reduction with fixed RF-contacts (b).

simulations [8] give a clear indication about the need of shielding the VFs and reduce the current contribution to the longitudinal beam impedance. The effect of shielded VFs, however, is visible in simulations for intensity threshold only if other measures are applied in addition. Most important in this respect are the HOMs resulting from the 200 MHz TWC,

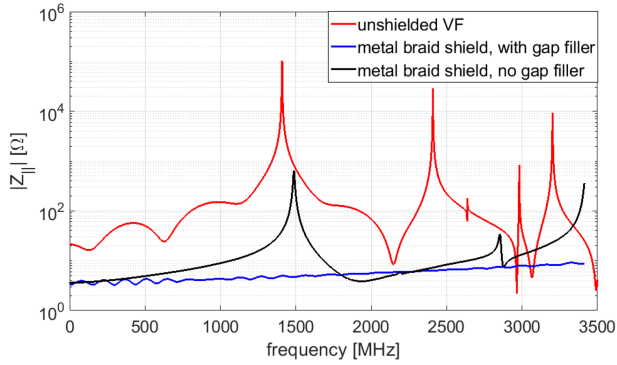


Figure 3: Comparison of simulation results for the longitudinal impedance contribution of one SPS vacuum flange connecting an MBA beam-pipe to a QF beam-pipe. Red: unshielded VF, black: VF equipped with braided shield, blue: VF equipped with braided shield and modified gasket (gasket gap filled). The closing of the flat unintended cavity at the gasket location suppresses the remaining resonance at about 1.5 GHz.

where currently a HOM-reduction factor of 2 to 3 is targeted and appears reachable [9]. Note that these simulations [7] were performed for the situation with 72 bunches in the SPS after an RF-upgrade on the 200 MHz TWC to reach a total accelerating voltage of 10 MV. As can be seen in Fig. 4, for a HOM-reduction in the 200 MHz cavity of a factor of three, an additional 10 % can be gained by shielding the VFs.

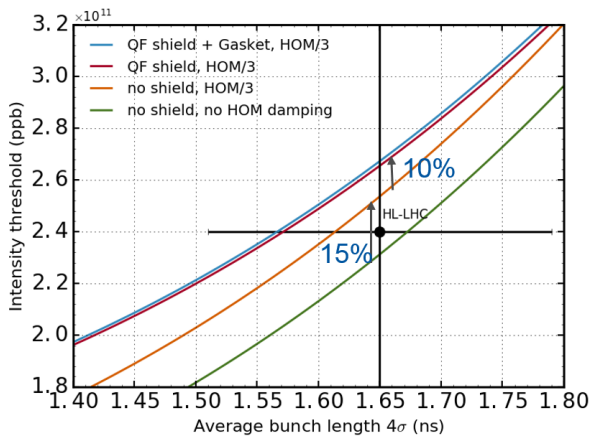


Figure 4: Simulation results for intensity threshold on the SPS 450 GeV/c flat top with 72 bunches spaced by 25 ns for an RF-voltage of 10 MV at 200 MHz and 1 MV at 800 MHz. The simulation compares the situation of shielded and unshielded vacuum flanges connecting an MBA-type beam-pipe to an elliptical QF-type beam pipe. Courtesy of J. Repond [8].

UHV Gate Valve of PS (Example 2)

In the framework of the development of an impedance model for the CERN Proton Synchrotron (PS), priority was given to the modeling of machine elements of which the

contribution to the overall beam impedance is known to be significant as, e.g. the accelerating cavities, and the kickers. However, smaller passive machine parts like the ultra-high vacuum (UHV) gate valves or beam pipe bellows equally have to be modelled as these are expected to contribute due to the large number of elements installed in the PS. For the PS UHV gate valves, a simplified impedance model existed for the calculation of transverse impedance. This model mainly represented the integrated dimensions of the structure since due to proprietary rights of the manufacturer, no geometrical model exists of this structure. We have therefore taken assumptions on the mechanical part inside the outer body of the gate valve. It could be shown from simulations, that leaving out these parts will result in an entirely different impedance contribution, i.e. to a misleading interpretation of the longitudinal impedance. Fig. 5 shows the previous impedance model (a), and the modified geometry (b) including the mechanical part.

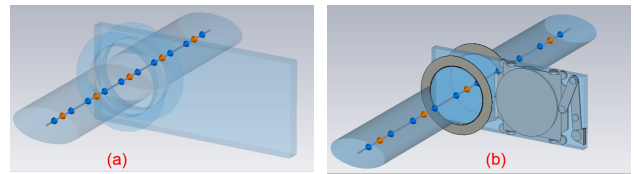


Figure 5: PS UHV geometrical gate valve models. Simplified geometry (a), and improved model including the inner parts that represent the valve mechanism (b).

Due to lack of geometry knowledge, the simulation model of the PS UHV valves had to be benchmarked by means of EM-measurements to ensure that the assumed geometry correctly represents its main features with respect to beam impedance. For this purpose, we connected RF-pipes on both sides of the valve such that EM-measurements with a vector network analyser could be carried out by inserting capacitively coupling coaxial RF-probes. It should be noted that a direct connection of measurement probes to the valve is not possible as this would have a strong effect on the resonances since in the main body of the valve, coupling could not be sufficiently reduced. The RF-probes are inserted on-axis into the connected beam pipes to detect resonances from transmission measurements. In all cases, it has been assured that only a weak coupling of the probe to the valve's resonance of less than approx. 100 mdB took place in order to avoid a falsification of the measurement trace.

Fig. 6 shows the comparison of simulated transmission measurements obtained from the model in CST [10] (dashed lines) and the measured traces for the three most significant resonances at approx. $f_{res} = 1207$ MHz, 1346 MHz, and 1504 MHz that could be excited with the centered probe positions. Eigenvalues have been calculated with the beam pipes terminated by short planes to allow additional cross-checks of the resonance frequencies.

As can be seen from the comparison of the traces, the measured resonances of TE_{111} (at 1.207 GHz) and TE_{116} (at 1.346 GHz) could be precisely reproduced from the sim-

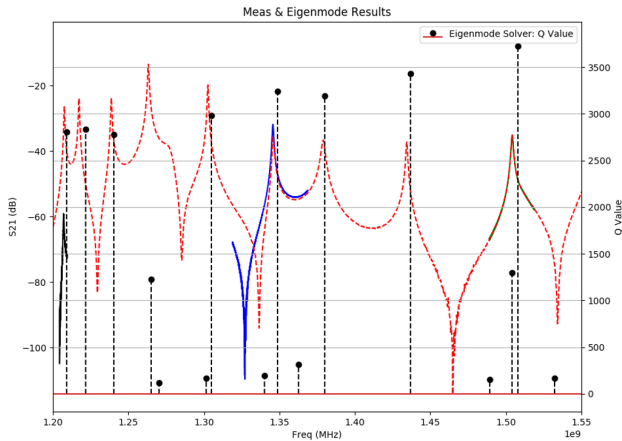


Figure 6: PS UHV gate valve: Comparison between simulations (both Eigenmode and transmission solver results) and measurements taken with a VNA using coaxial RF-probes.

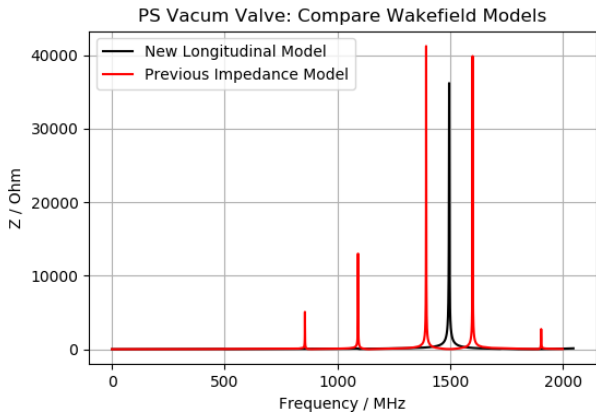


Figure 7: Simulated longitudinal beam impedances as obtained from an oversimplified valve geometry, and a more precisely modeled valve containing the inner mechanism.

ulated transmission, as well as the resonance frequency of TM_{010} (at 1.504 GHz). Note that the TM_{010} is at a higher frequency than the two TE-modes resulting from the change of the resonator geometry by adding the beam pipes. It should also be mentioned that the selected measurement set-up restricts the positioning of the measurement probes onto the beam axis. Consequently, due to the resulting field configuration, only a limited number of the modes that are truly resonating in the valve can be excited. The good reproduction of the three peaks, however, give sufficient confidence in the correct reproduction of the valve's geometry for impedance calculation. Fig. 7 shows the calculated longitudinal impedance obtained from the earlier simplified geometry (shown in Fig. 5 (a)) compared to the improved longitudinal model (Fig. 5 (b)) from which a longitudinal beam impedance contribution of about 36 k Ω could be attributed to one valve. In total, there are 10 valves of this type used in the PS.

Kicker Magnet (KFA45) of PS (Example 3)

The fast kickers of the PS like the so-called KFA45, consist of a variable number of magnet modules contained in one common vacuum tank. Each of these magnet modules is geometrically built of intersecting parts of alternating aluminum plates and ferrite sections that are supported within an aluminum framework. These ferrites must be modeled accurately, since they behave as attenuators at lower frequencies, whereas at higher frequencies, they become transparent.

A multitude of modes are supported by the ferrites and the spacing between the plates. Additionally, due to the close proximity of these sections heavy coupling between the modes in the modules takes place. Further modes are observed within the vacuum tank itself; these are supported by the framework of the modules and the plate-ferrite sections.

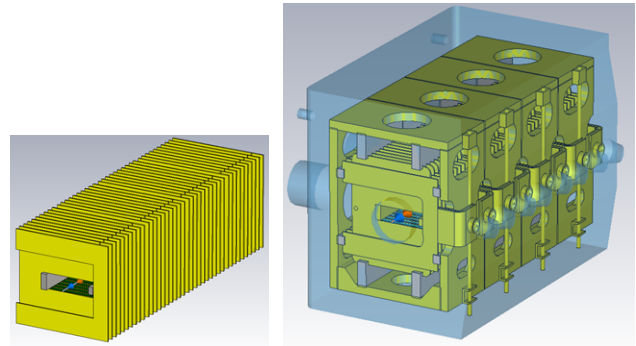


Figure 8: Models of the geometry of the fast kickers, simplified model (left) and complete model (right), shown to scale.

Previous work [11] in the transverse impedance domain resulted in a simplified model of the kicker that does not include the framework of the kicker, neither its vacuum tank (as is shown in Fig. 8 (left)). This model was used as a starting point to build a more complete geometry required as input for the longitudinal impedance model of the PS (see Fig. 8 (right)), which incorporates the complete geometry of the kicker.

Due to the large amount of modes present in the kicker, eigenmode analysis was impossible and also could even be misleading, since many modes are broadband with frequencies close to one another, such that they would 'stack' upon one another. Consequently, they cannot be analyzed independently. As a result, only wakefield simulations give reasonable results for these types of objects. As an example, the transverse model was simulated for the longitudinal impedance and is compared with the complete model's longitudinal impedance in Fig. 9

Of particular note is the resonance peak at 600 MHz obtained from the simplified model which shifts as low as 60 MHz for the complete model. Further study of the field distributions showed that this shift is the direct result of this mode resonating in the free space around the ferrite-plate sections. The complete kicker model provides for the added

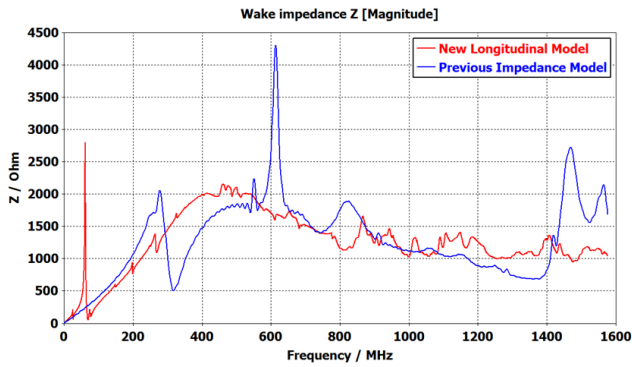


Figure 9: Comparison of calculated wakefields resulting from previous, simplified impedance model and new, complete impedance model of the KFA45.

space in these sections thus pushing this resonance to lower frequency due to its larger overall volume. Note that the overall longitudinal impedance for both models, except for the peak, is very broadband.

Reworking of a Machine Section (Example 4)

In the framework of the ongoing impedance reduction efforts taken for the SPS, each new machine element to be installed into the accelerator has to undergo an impedance evaluation that makes part of an installation approval process. This evaluation includes the calculation of the direct surroundings in the machine to determine if additional elements, like e.g. beam-pipe tapers or other mitigating parts are required. In many cases, impedance shields for the new machine element can be suggested and are implemented. However, in this way, not only individual machine elements could be identified to which a large contribution to beam impedance was attributed, but also some groups of different machine components stood out with a noticeable impedance contribution which resulted from repeated change of beam pipe cross-sections. Further study of these machine sections showed that their overall impedance could not simply be reproduced by adding up the individual contributions of its elements. Instead, wakefield calculations for the entire area had to be carried out as one geometry to obtain a correct impedance contribution, making these simulations heavy and time-consuming. It could be observed that the repetition of a large number of cross-sectional changes from narrow beam-pipe to larger beam-pipe cross-sections results in a cavity-like behaviour of some elements, explicitly in the case of round bellows due to their pill-box shape. This is, however, only the case if the bellow is installed with a narrow beam pipe on both sides. Otherwise, the same bellow does not resonate cavity-like, but contributes with its longitudinal size to the adjacent machine element as a volume extension. Fig. 11 (top) shows the original layout of such an area in the SPS where upstream of a corrector magnet, a large number of cross-sectional changes of the beam pipe could be found. The area consists of different machine elements starting with a beam position monitor (so-called BPCE) with circular aperture that is followed by a small corrector dipole (so-called

MDHA) which is clamped around an elliptical beam pipe of 156 mm width (QFA-type). Three large aperture bellows of two different types are required to allow alignment of the machine elements and to flange the different beam pipe apertures. It should be noted that work in these areas was not foreseen within impedance reduction programmes so far, however, the request of installation of an additional machine element with a race-track shaped aperture upstream of the BPCE led to this investigation of the entire area. Fig. 11 (bottom) also shows the top view and the side view of the original layout as modelled in CST [10]. The location where the new machine element with a race-track shaped aperture is to be inserted into the existing accelerator structure is also indicated. The original layout is with a round beam-pipe at this location.

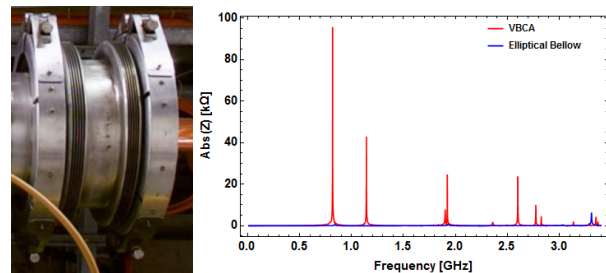


Figure 10: Left: VBCA bellow type consisting of two undulated parts that are connected via a large round opening. Right: Simulated longitudinal beam impedance for the VBCA bellow compared to an elliptical bellow with same horizontal aperture.

The two bellow types are denoted VBDA for the standard bellow and VBCA for the bellow with two separated undulations of which two are used in this area. Fig. 10 (left) shows the VBCA bellow that consists of two undulated parts that are resonating individually and a straight part acting as a large opening that allows full coupling of the resonances which are building up in the bellow undulations. The VBCA bellow has an inner diameter of 340 mm and ends in DN273 flanges, and its main contribution to longitudinal beam impedance could be identified at about 850 MHz, if it is connected on both sides with elliptical beam pipes. This is the case for the bellow position just upstream of the QFA, however, not for the second identical bellow that is located downstream of the BPCE.

It would therefore be incorrect to just calculate the longitudinal beam impedance of the VBCA bellow with elliptical beam pipes on both sides and then double its contribution. Fig. 10 (right) shows the contributing longitudinal impedance of this bellow compared to an elliptical bellow of the same mechanical functionality. From simulation, a contribution of about 90 kΩ is obtained for the VBCA connected to elliptical beam pipes on both sides, in addition to a number of other modes for frequencies above 1 GHz, resulting from the fact that this bellow is shaping an unintended cavity with resonator-behaviour. Note that in this location, mainly elliptical beam-pipes are used, hence aperture re-

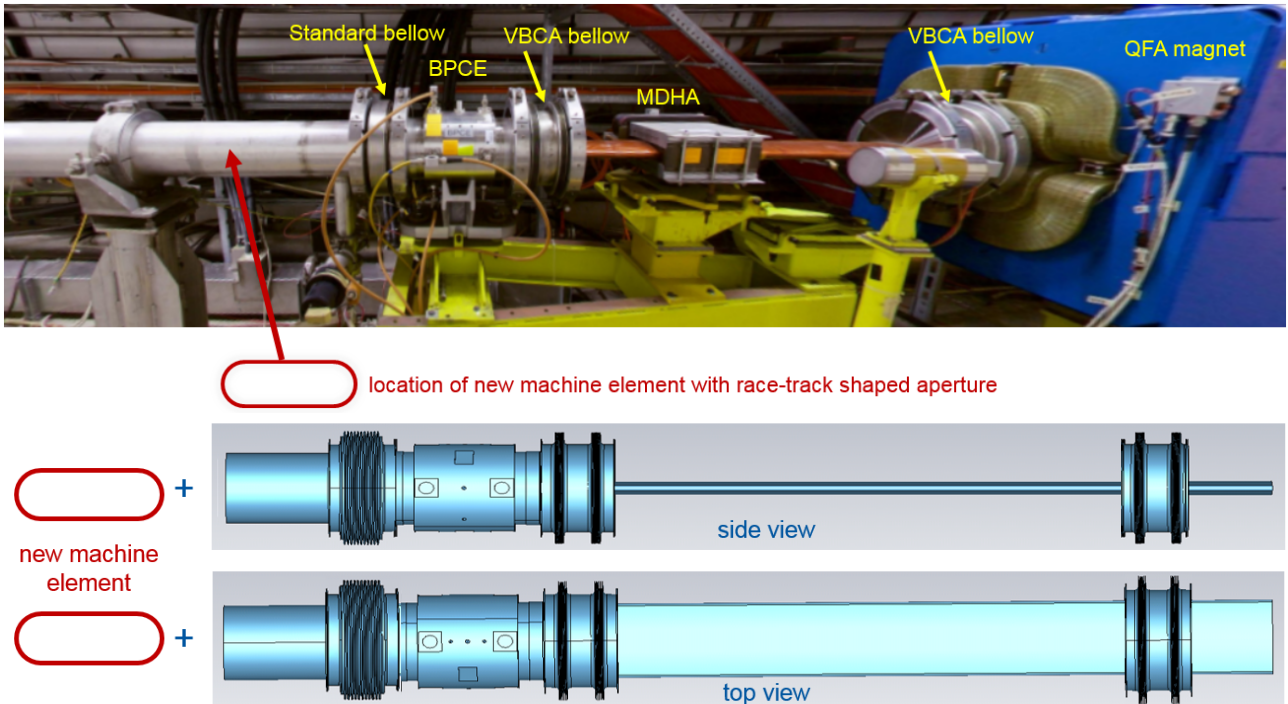


Figure 11: Top: Picture of the original layout of the SPS area for evaluation for impedance improvement due to sorting. Bottom: Top view and side view of the original layout as modelled in CST [10] where the race-track shaped aperture shall be inserted into the existing round beam pipe upstream of the BPCE with its adjacent large aperture standard bellow.

quirements allow for the exchange of VBCA and VBDA bellows with large round apertures with elliptical bellows of the same horizontal aperture. Fig. 12 shows the simulated

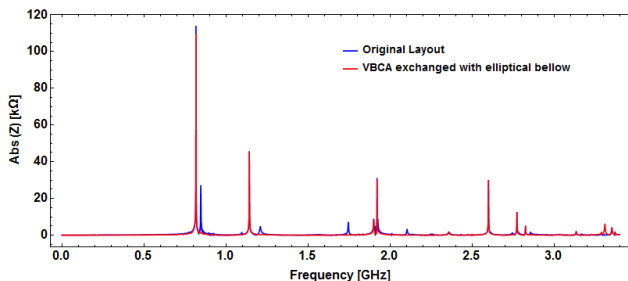


Figure 12: Simulated longitudinal beam impedance obtained from the original layout (blue trace) and after the exchange of the VBCA bellow with an elliptical bellow (red trace).

longitudinal beam impedance obtained from the original layout (blue trace) and after the exchange of the VBCA bellow with an elliptical bellow (red trace). As expected, the peak at approx. 850 MHz vanishes when the VBCA bellow next to the quadrupole is removed. Note that only the VBCA bellow next to the quadrupole magnet was removed, whereas the second VBCA bellow, located downstream of the BPCE is still in the layout. As was mentioned before, the VBCA bellow is contributing differently, depending on how it is flanged on at both sides. In this case, the VBCA bellow downstream of the BPCE is simply acting as a volume extension for the position monitor, and is not acting as an unwanted cavity by creating narrowband resonances.

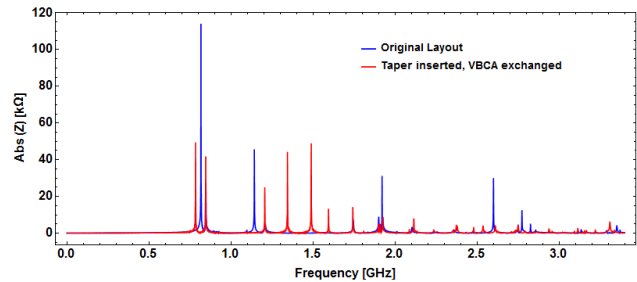


Figure 13: Simulated longitudinal beam impedance obtained from the original layout (blue trace) and after the insertion of an ideal taper to provide transition from the race-track shaped aperture to a round one. In addition, the VBCA bellow was exchanged for an elliptical bellow (red trace).

As a next step, a taper was inserted in the simulations to provide a smooth continuity between the new machine element with its race-track shaped aperture and the existing structure with a round aperture. Today, the use of individualised tapers is standard in most accelerators, following the rule-of-thumb to only keep a minimum number of steps along the vacuum chamber. The taper in our case was calculated as ideal transition from the race-track shaped aperture to round aperture. In addition, one elliptical bellow was placed upstream of the taper, replacing the VBCA. Fig. 13 shows the resulting simulated longitudinal impedance of this study (red trace) compared to the original layout (blue trace). It can be seen that by inserting the taper, resonances at about 1.15 GHz and 1.9 GHz, as well as some higher frequency resonances were suppressed compared to the original layout. However, the largest resonance at about 850 MHz does not

vanish, but is instead reduced by about half and split in two individual resonances. In addition, a number of new resonances shows up in the frequency range between 1 GHz and 2 GHz which diminish the overall improvement. It was then decided to evaluate a possible sorting of the existing machine elements. For this purpose, the VBCA bellow upstream of the quadrupole magnet was exchanged with an elliptical bellow, and the positions of the new machine element and the BPCE with the two connected bellows were swapped. Note that this action moves the BPCE further away from the QF, a change in layout that had first to be agreed by operations to confirm that the functionality of the BPCE is not compromised. Fig. 14 shows the simulated longitudinal beam impedance obtained after sorting the machine elements for best impedance performance (red trace), and compared to the original layout (blue trace). As can be seen from the plots, sorting of the machine elements led to a considerable reduction of the longitudinal beam impedance over the entire frequency range with maximum narrowband contributions of less than 10 k Ω longitudinal beam impedance at about 800 MHz, 1.9 GHz and above 3 GHz which can be considered entirely negligible within the overall impedance budget of the accelerator.

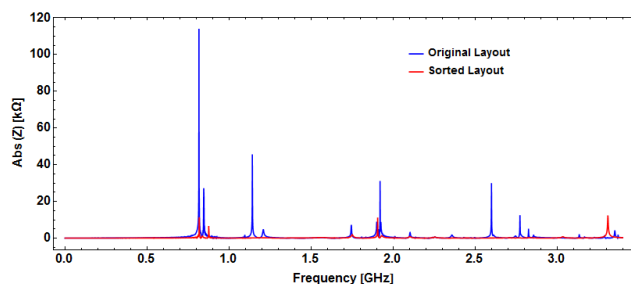


Figure 14: Simulated longitudinal beam impedance obtained from the original layout (blue trace) and after sorting the individual machine elements for best impedance performance (red trace).

CONCLUSION

In this contribution, we investigated the longitudinal beam impedance contribution of various machine elements and possible solutions for their mitigation by means of worked examples. We looked at narrowband and broadband impedances and gave examples of possible mitigations for individual machine elements. One major source of contribution are cross-sectional changes of the beam pipe aperture, hence impedance shields that provide a smooth transition between different beam pipe shapes are an effective way to improve the impedance contribution. It was further shown that considerable care has to be given to the geometrical modeling of individual machine elements in order to correctly reproduce their EM-behaviour. Explicitly elements that appear to be mechanically simple such as flanges, bellows and valves can be electromagnetically complex. It was shown with the example of the PS UHV sector valve, that for machine elements in existing accelerators, where no good mechanical description is available, RF-measurements of

the element are required to benchmark the simulation model. With the example of a kicker magnet, it was demonstrated how over-simplifications of the geometrical model can lead to misinterpretation of the calculated beam impedance contribution. Further, with the example of the VBCA bellows, it was also shown that special care is required in counting the number of machine elements and multiplying the individual contribution without considering the installation situation. Finally, we demonstrated that besides the improvement of individual machine elements, also sorting of their positions in the lattice should be considered if the layout allows for this, since sorting can give an impedance improvement of the overall section without modifying the individual machine elements.

REFERENCES

- [1] E. Shaposhnikova *et al.*, “Removing Known SPS Intensity Limitations for High Luminosity LHC Goals”, in *Proc. of Int. Particle Accelerator Conf. (IPAC’16)*, Busan, Korea, May 2016, paper MOPOY058, pp. 989–991.
- [2] J. E. Varela, “Longitudinal Impedance Characterization of the CERN SPS Vacuum Flanges”, in *Proc. of Int. Particle Accelerator Conf. (IPAC’15)*, Richmond, VA, USA, May 2015, paper MOPJE036, pp. 363–365.
- [3] J. Perez-Espinos, *et al.*, “Analysis and Testing of a New RF Bridge Concept as an Alternative to Conventional Sliding RF-Fingers in the LHC”, in *Proc. of Int. Particle Accelerator Conf. (IPAC’16)*, Busan, Korea, May 2016, paper THPMY006, pp. 3660–3662.
- [4] Ogiwara, *et al.*, “Ultrahigh Vacuum for High Intensity Proton Accelerators: Exemplified by the 3 GeV RCS in the J-Parc”, in *Proc. of Int. Particle Accelerator Conf. (IPAC’11)*, San Sebastian, Spain, May 2011, paper TUZB02, pp. 971–975.
- [5] Ogiwara, *et al.*, “Bellows with a New RF Shield Made of Metal Braid for High Intensity Proton Accelerators”, in *Proc. of Int. Particle Accelerator Conf. (IPAC’13)*, Shanghai, China, May 2013, paper THPF1014.
- [6] T. Kaltenbacher, *et al.*, “Characterization of Shielding for the CERN-SPS Vacuum Flanges With Respect to Beam Coupling Impedance”, in *Proc. of Int. Particle Accelerator Conf. (IPAC’17)*, Copenhagen, Denmark, May 2017, paper WEPIK090, pp. 3143–3146.
- [7] BLonD, Beam Longitudinal Dynamics code, <http://blond.web.cern.ch/>.
- [8] J. Repond, *et al.*, “Effect of HOM frequency shift on bunch train stability”, *these proceedings*, Benevento, Italy, September 2017.
- [9] P. Kramer, *et al.*, “Studies for the SPS Travelling Wave Cavities Upgrade”, *these proceedings*, Benevento, Italy, September 2017.
- [10] CST AG, Darmstadt, Germany, <http://www.cst.com/>.
- [11] S. Persichelli *et al.*, “The transverse beam coupling impedance of the CERN Proton Synchrotron” in *Phys. Rev. Accel. Beams*, vol. 19 no. 4, p.041001, April 2016.